Role of epitaxy in controlling the magnetic and magnetostrictive properties of cobalt ferrite–PZT bilayers

2010 J. Phys. D: Appl. Phys. 43 485001

(http://iopscience.iop.org/0022-3727/43/48/485001)

IOP PUBLISHING JOURNAL OF PHYSICS D: APPLIED PHYSICS

J. Phys. D: Appl. Phys. **43** (2010) 485001 (8pp) doi:10.1088/0022-3727/43/48/485001

Role of epitaxy in controlling the magnetic and magnetostrictive properties of cobalt ferrite–PZT bilayers

D Mukherjee, T Dhakal, R Hyde, P Mukherjee, H Srikanth and S Witanachchi

Department of Physics and Center for Integrated Functional Materials (CIFM), University of South Florida, Tampa, FL 33620, USA

E-mail: switanach@usf.edu

Received 26 July 2010, in final form 4 October 2010
Published 16 November 2010
Online at stacks.iop.org/JPhysD/43/485001

Abstract

Epitaxial thin films of cobalt ferrite (CFO) single layer and CFO–lead zirconium titanate (PZT) bilayers were deposited on single crystal MgO (1 0 0) and $SrTiO_3$ (STO) (1 0 0) substrates by pulsed laser deposition. The structural properties were characterized using x-ray diffraction and atomic force microscopy. The magnetic properties of the as-grown thin films were measured at 10 and 300 K in both parallel and perpendicular magnetic fields. The CFO–PZT bilayer films showed enhanced or reduced values of magnetization as compared with those of the CFO single layer films depending on the substrate of deposition. A strain compression–relaxation mechanism was proposed in order to explain the structure–property relationships in the CFO–PZT bilayer thin films.

(Some figures in this article are in colour only in the electronic version)

1. Introduction

Magnetostriction is a well-known property of magnetic materials associated with the change in dimensions upon magnetization [1, 2]. As a result, elastic strains are developed in the crystal lattice that change the alignment of the magnetic moments and create the magnetoelastic effect in the material [3, 4]. Cobalt ferrite, $CoFe_2O_4$ (CFO), belongs to the family of spinel-type ferrites and is one of the important magnetic materials with high coercivity, moderate magnetization and highest magnetostriction coefficient ($\lambda_{100} = -200 \times 10^{-6}$ to -590×10^{-6}) [1, 5]. CFO has been extensively explored as a promising magnetostrictive material for applications in actuators, sensors and transducers [6–9]. It is also considered as a key component for multiferroic multilayers or composites [10]. When coupled with ferroelectric materials such as $BaTiO_3$ (BTO) or $Pb(Zr,Ti)O_3$ (PZT), CFO exhibits the magnetoelectric (ME) effect [11, 12]. From an industrial perspective such horizontal heterostructures of ferromagnetic and ferroelectric materials have potential applications as ME memory devices [13]. So far, there are numerous reports on ME effect in layered CFO–PZT structures mostly grown on $Pt/Ti/SiO_2/Si$ substrates [14–19] and only a few on MgO or STO substrates [20, 21]. The residual strain at the CFO–PZT interface is the dominating factor that dictates the ferromagnetic properties in epitaxial CFO–PZT thin films [22, 23]. This suggests that 'strain engineering' is an important aspect in these ferroelectric/ferromagnetic structures. However, structural parameters that quantify this behaviour have remained elusive. Hence a systematic study on the role of epitaxy in controlling the magnetic properties of CFO–PZT bilayer films would be beneficial.

In this work, epitaxial thin films of CFO single layer and CFO–PZT bilayers were grown on single crystal MgO and $SrTiO_3$ (STO) substrates by pulsed laser deposition (PLD). The magnetic properties of the as-grown thin films were measured at 10 and 300 K by applying magnetic fields both parallel and perpendicularly to the film planes. The CFO–PZT bilayer films showed enhanced or reduced values of magnetization as compared with that of the CFO single layer films depending on the substrate of deposition. A strain compression–relaxation mechanism has been proposed in order to explain the structure–property relationships in the CFO–PZT bilayer thin films.

An increase in the residual stress due to the top PZT layer on the CFO layer and its effect on magnetization has been reported earlier on the polycrystalline films grown on silicon [15]. Sim *et al* had suggested that the residual stress in the CFO films on Si could be intrinsic and associated with the orientation change or defect incorporation or non-equilibrium phase formation. However, the stress mechanisms were complicated and difficult to quantify [15]. In this work the residual stress could be estimated due to epitaxial growth. The investigation may provide a comprehensive direction towards tailoring the magnetic anisotropy of CFO epitaxial thin films for potential device applications.

2. Experimental

The Pulsed Laser Deposition (PLD) technique was adopted to grow the epitaxial CFO single layer and bilayer thin films on 1 cm × 0.5 cm single crystalline MgO (1 0 0) and $SrTiO_3$ (STO) (1 0 0) substrates. Henceforth, the nomenclature CFO/MgO and CFO/STO for CFO single layer thin films on MgO and STO substrates, respectively, will be used in the text. Similarly, the CFO–PZT bilayer thin films grown on MgO and STO substrates will be referred to as PZT/CFO/MgO and PZT/CFO/STO, respectively. The deposition chamber was attached to a custom-built multi-target holder that allowed for the *in situ* deposition of multilayers with clean interfaces. A distance of 6 cm was maintained between the substrates and the targets during deposition. Compressed powder targets of CFO and $Pb(Zr_{0.52}Ti_{0.48})O_3$ were ablated using a KrF excimer laser ($\lambda = 248$ nm) operating at 10 Hz. All the films were deposited with an energy density of 2 J cm^{-2} at the target surface. For the PZT/CFO/MgO and PZT/CFO/STO thin films, the CFO layer was deposited at 450 °C, 10 mTorr O_2 pressure and at an average deposition rate of 0.1 Å/pulse. A 200 nm layer thickness was achieved through these parameters. The subsequent PZT layer of the same thickness was deposited at 550 °C, 300 mTorr O_2 pressure. The CFO/MgO and CFO/STO films of similar thicknesses were prepared under the same experimental conditions for comparison. The crystallinity and the in-plane epitaxy of the deposited thin films were confirmed by θ–2θ scans, rocking curve analysis and φ (azimuthal) scans using x-ray diffraction (XRD) (Bruker D 8 Focus and Philips X'pert Diffractometer). Peak shifts due to sample misalignment were taken care of while performing the XRD scans. The surface morphologies were studied using an atomic force microscope (AFM, Digital Instruments). The magnetization measurements of the thin films were performed using a commercial Physical Property Measurement System (PPMS) from Quantum design.

3. Results and discussion

3.1. Crystallinity and surface morphology

The small lattice mismatch (0.04%) between PZT (tetragonal perovskite, lattice parameters, $a = b = 4.036$ Å, $c = 4.146$ Å) [24] and CFO (face-centred cubic (fcc), lattice parameter, $a = 8.391$ Å) [25] as well as between CFO and the substrates

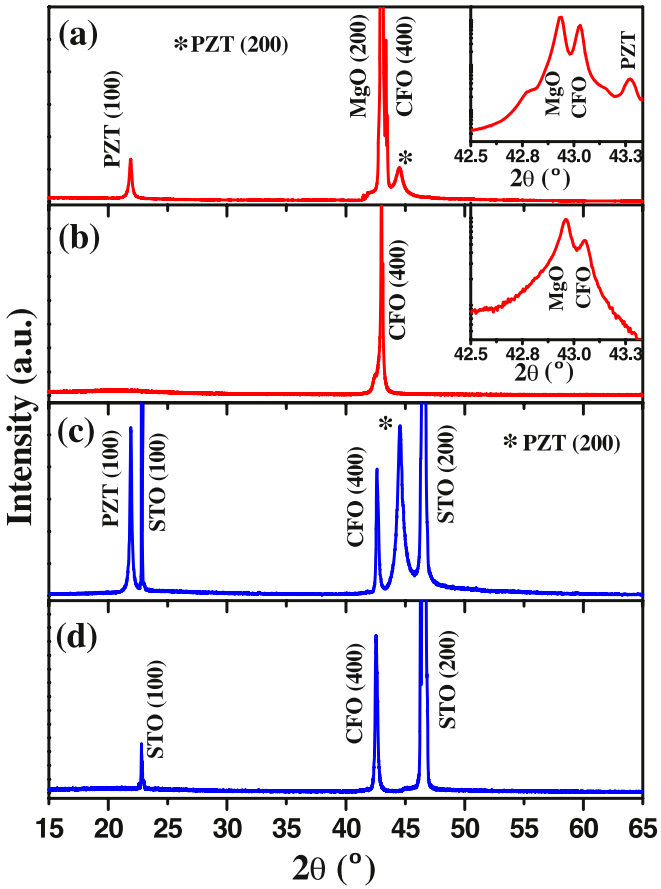

Figure 1. XRD θ–2θ scans for single layer CFO and bilayer CFO–PZT films grown on MgO (*a*) and (*b*) and STO substrates (*c*) and (*d*), respectively. The insets to (*a*) and (*b*) show the details of the MgO (2 0 0), CFO (4 0 0) and PZT (2 0 0) peaks around 43°.

allowed for the growth of the epitaxial films. Figures 1(*a*) and (*b*) show the XRD θ–2θ spectra for PZT/CFO/MgO and CFO/MgO, respectively. The XRD spectra for PZT/CFO/STO and CFO/STO are shown in figures 1(*c*) and (*d*), respectively. In all the samples the single phase nature and epitaxial relationship with the substrates were observed. The XRD peak in CFO was assigned to the (4 0 0) plane, corresponding to the fcc phase of CFO with space group *Fd*-3*m* (2 2 7). For PZT/CFO/MgO and PZT/CFO/STO films, the PZT peak was indexed to the (1 0 0) plane of tetragonal PZT with space group *P*4*mm* (99) (figure 1(*a*) and (*c*)). Due to the small lattice mismatch between MgO (fcc, 2 × lattice parameter = 8.42 Å) [26] and CFO, the MgO (2 0 0) and CFO (4 0 0) peaks were in close occurrence to each other in the θ–2θ spectra. The insets to figures 1(*a*) and (*b*) visibly show the MgO and CFO peaks in the samples. However, due to the larger lattice mismatch between STO (primitive cubic, 2 × lattice parameter = 7.81 Å) [27] and CFO, the (4 0 0) peaks of CFO were shifted significantly (figures 1(*c*) and (*d*)) as compared with the peaks of polycrystalline CFO [25]. The out-of-plane lattice parameter ($a_\perp$) for CFO was calculated from the XRD θ–2θ scans (see table 1).

In order to verify the in-plane epitaxial relationship and cubic symmetry for the CFO and PZT layers, φ scans were performed. Figures 2(*a*) and (*b*) show the φ scan

Table 1. FWHM of rocking curves about the CFO (4 0 0) plane, in-plane ($a_\parallel$) and out-of-plane ($a_\perp$) lattice parameters obtained from XRD peaks, in-plane ($\varepsilon_\parallel$) and out-of-plane ($\varepsilon_\perp$) strains calculated using $\varepsilon = (a - a_o)/a_o$, where a is $a_\parallel$ or $a_\perp$ and a_o is the bulk lattice parameter of CFO ($a_o = 8.39$ Å), and the in-plane stress calculated from in-plane strain and Young's modulus of CFO ($Y = 1.5 \times 10^{12}$ dyn cm^{-2}) for CFO and CFO–PZT films on MgO and STO substrates.

Sample	FWHM of rocking curve (°)	$a_\perp$ (Å)	Out-of-plane strain ($\varepsilon_\perp$)	$a_\parallel$ (Å)	In-plane strain $\varepsilon_\parallel$	In-plane stress $\times 10^9$(dyne cm^{-2})
CFO/MgO	0.076	8.386	−0.0005	8.403 ± 0.004	0.0015 ± 0.0005	2.3 ± 0.6
PZT/CFO/MgO	0.321	8.338	−0.0062	8.294 ± 0.007	−0.0114 ± 0.0008	−17.1 ± 0.1
CFO/STO	0.915	8.494	0.0124	8.292 ± 0.005	−0.0116 ± 0.0006	−17.5 ± 0.09
PZT/CFO/STO	0.986	8.479	0.0106	8.330 ± 0.002	−0.0071 ± 0.0002	−10.7 ± 0.03

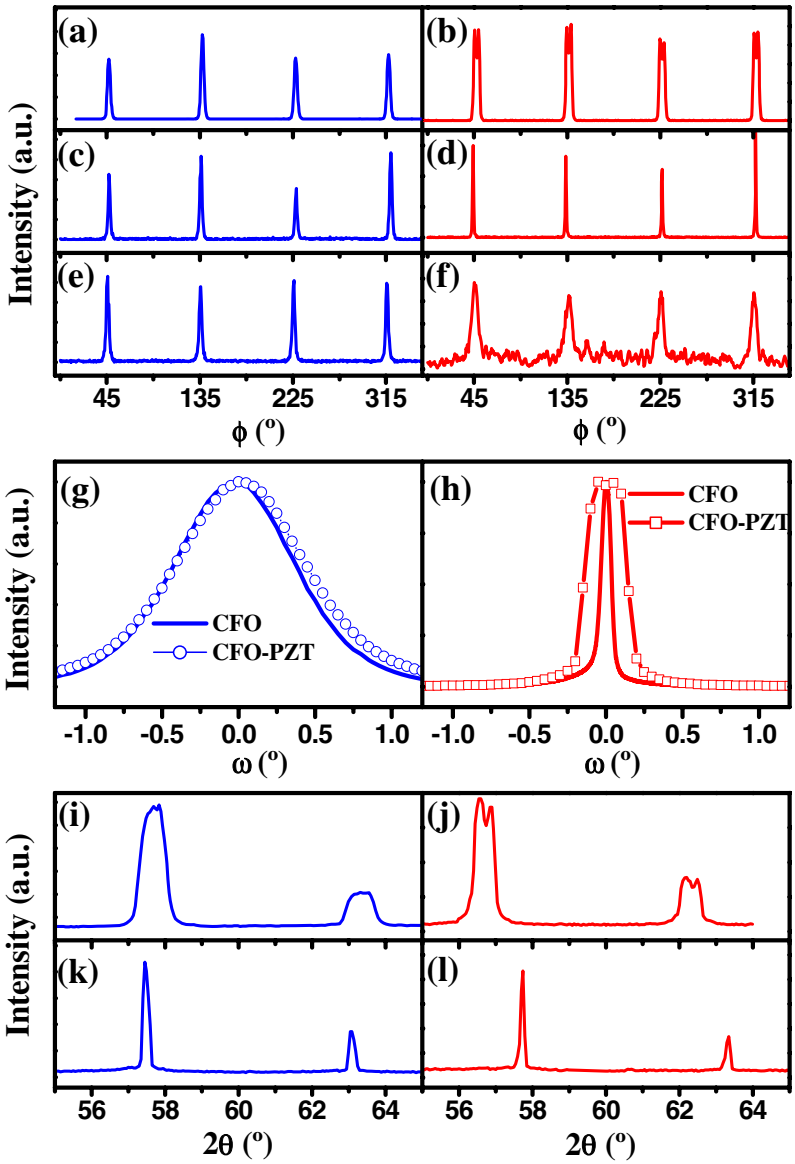

Figure 2. Left and right columns represent the films grown on STO and MgO substrates, respectively. (*a*) and (*b*) are φ scan spectra from PZT (1 0 1) reflection in CFO–PZT bilayer film. (*c*) and (*d*) and (*e*) and (*f*) are φ scan spectra from (3 1 1) CFO reflection in CFO–PZT bilayer and single layer CFO films respectively. (*g*) and (*h*) are rocking curves of CFO (4 0 0) peaks. (*i*) and (*j*) and (*k*) and (*l*) are asymmetric scans of (5 1 1) and (4 4 0) CFO planes for single layer CFO films and bilayer layer CFO–PZT films, respectively. (*i*)–(*l*) Left peaks are from the CFO (5 1 1) plane and the right peaks are from CFO (4 4 0) planes.

spectra from the PZT (1 0 1) plane for PZT/CFO/STO and PZT/CFO/MgO, respectively. Figures 2(*c*) and (*d*) show the φ scan spectra from the CFO (3 1 1) plane for PZT/CFO/STO and PZT/CFO/MgO, respectively. Figures 2(*e*) and (*f*) show the φ scan spectra from the CFO (3 1 1) plane for CFO/STO and CFO/MgO, respectively. In all cases, the peaks in the φ spectra occurred at intervals of 90° suggesting the four-fold cubic symmetry and cube-on-cube growth. Figures 2(*g*)

and (h) show the rocking curves (ω scans) about the CFO (4 0 0) planes for PZT/CFO/STO and CFO/STO, and PZT/CFO/MgO and CFO/MgO, respectively. The small full-width at half maximum (FWHM) values ($<1^\circ$) of the rocking curves confirmed a good degree of in-plane orientation for CFO in all the samples (see table 1 for FWHM values). However, the (4 0 0) texture was sharper in the films grown on MgO which may be attributed to the smaller lattice mismatch between CFO and MgO. In addition, the degree of (4 0 0) texturing of CFO weakened slightly in PZT/CFO/STO and PZT/CFO/MgO compared with PZT/STO and PZT/MgO, respectively. Figures 2(i) and (j) show the asymmetric scans of the (5 1 1) and (4 4 0) planes of CFO for CFO/STO and CFO/MgO, respectively. Figures 2(k) and (l) show the similar asymmetric scans for PZT/CFO/STO and PZT/CFO/MgO, respectively. For figures 2(i) to (l) the left peaks are from the CFO (5 1 1) plane and the right peaks are from the CFO (4 4 0) planes. The average in-plane lattice parameters ($a_\parallel$) for CFO in the samples were calculated from the asymmetric scans shown in figures 2(i) to (l) (see table 1).

The strain (ε) in the CFO layer was calculated using the formula $\varepsilon = (a - a_o)/a_o$, where a is the out-of-plane ($a_\perp$) or in-plane ($a_\parallel$) lattice parameter and a_o is the bulk unstressed lattice parameter of CFO ($a_o = 8.39$ Å) [25]. Since the strain values depend sensitively on the lattice parameters the errors in measurements were estimated. The out-of-plane lattice parameters ($a_\perp$) for CFO were calculated by matching the 2θ values with respect to the substrate peaks which were considered unchanged. The errors in the in-plane lattice parameter ($a_\parallel$) measurements were calculated from the standard deviation of $a_\parallel$ values obtained from asymmetric scans about the CFO (5 1 1) and (4 4 0) planes (table 1). The in-plane stress ($\sigma_\parallel$) in the film was calculated using the relation $\sigma_\parallel = Y\varepsilon_\parallel$, where $\varepsilon_\parallel$ is the in-plane strain (ε) and Young's modulus value for CFO ($Y = 1.5 \times 10^{12}$ dyn cm^{-2}) [25]. Table 1 summarizes the lattice parameters and strains calculated for the out-of-plane and in-plane configurations.

From the strain values listed in table 1 it is seen that the CFO/MgO films grew with slight in-plane tensile ($\varepsilon_\parallel = 0.0015$) and out-of-plane compressive ($\varepsilon_\perp = -0.0005$) strains. On the other hand, the CFO/STO film grew with larger in-plane compressive ($\varepsilon_\parallel = -0.0116$) and out-of plane tensile ($\varepsilon_\perp = 0.0124$) strains. This could be attributed to the different lattice mismatches of CFO with MgO and STO substrates. The lattice mismatch at room temperature was calculated using the relation $(a_s - a_o)/a_s$ (%) where a_s is the lattice parameter of the substrate. The calculated values for CFO/MgO and CFO/STO were 0.36% and 7.8%, respectively. It was also observed that the in-plane lattice parameter ($a_\parallel$) of CFO for the PZT/CFO/MgO film ($a_\parallel = 8.294$ Å) was smaller than that of the CFO/MgO film ($a_\parallel = 8.403$ Å). This suggested that possibly with the deposition of the PZT layer on top, the CFO layer experienced an in-plane compression that compelled it to match its $a_\parallel$ to the smaller lattice parameter of PZT ($a = b = 4.036$ Å, $c = 4.146$ Å) [24]. As a consequence the in-plane strain and consequently the stress was amplified in PZT/CFO/MgO. However, an opposite trend was observed for the films grown on STO substrates. The CFO/STO film was already highly strained due to the large mismatch between the STO substrate and CFO. With PZT layer on top of it, the PZT/CFO/STO film was slightly relaxed to a lower strain state.

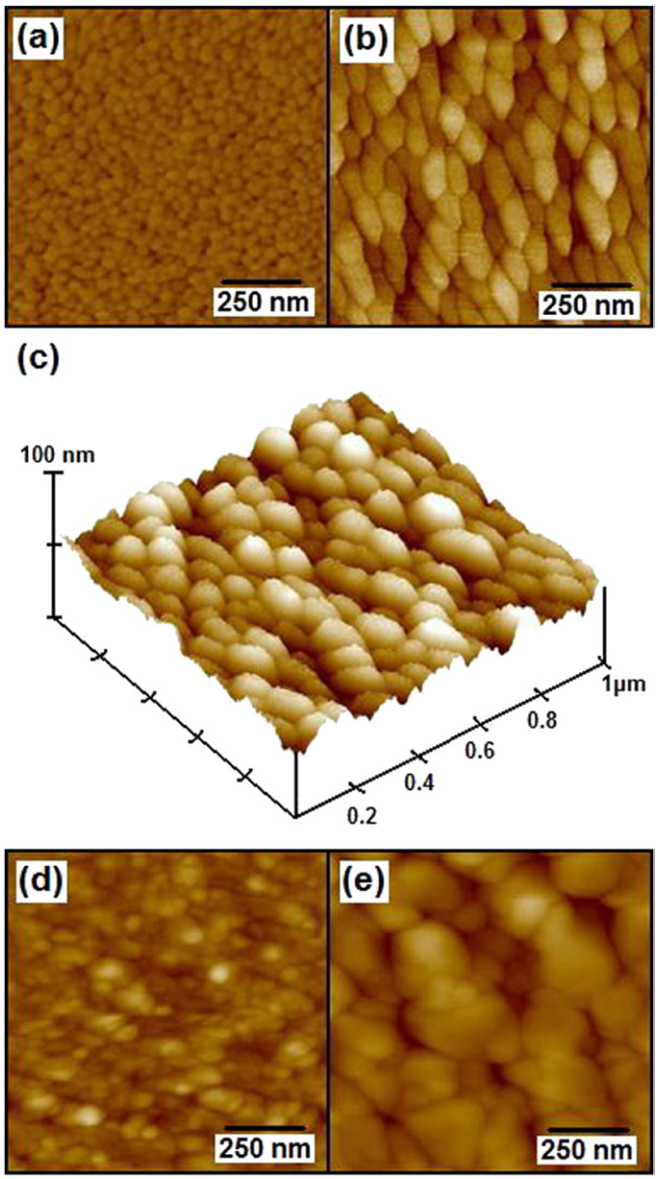

Figure 3. AFM images of (a) CFO surface of the CFO/MgO film, (b) top PZT surface of the PZT/CFO/MgO film, (c) 3D rendition of part (b), (d) CFO surface of the CFO/STO film and (e) top PZT surface of the PZT/CFO/STO films. Scan areas are $1 \times 1\ \mu m^2$ with z-height of 100 nm.

In order to analyse the surface morphologies of the thin films and predict their mechanisms of growth, AFM was employed. Figure 3(a) illustrates an AFM image of the CFO top layer for the CFO/MgO film. The image revealed a very smooth and compact surface with a root mean square roughness (R_{rms}) value of 2.084 nm and small grain size with relatively uniform size distribution similar to earlier reports [28, 29]. Figure 3(b) shows an AFM image of the PZT top layer for the PZT/CFO/MgO film. The PZT layer was relatively less smooth with R_{rms} value of 11.456 nm and larger grain size as compared with CFO/MgO. Uniform grain size distribution was also observed for PZT. The surface exhibited a texturing

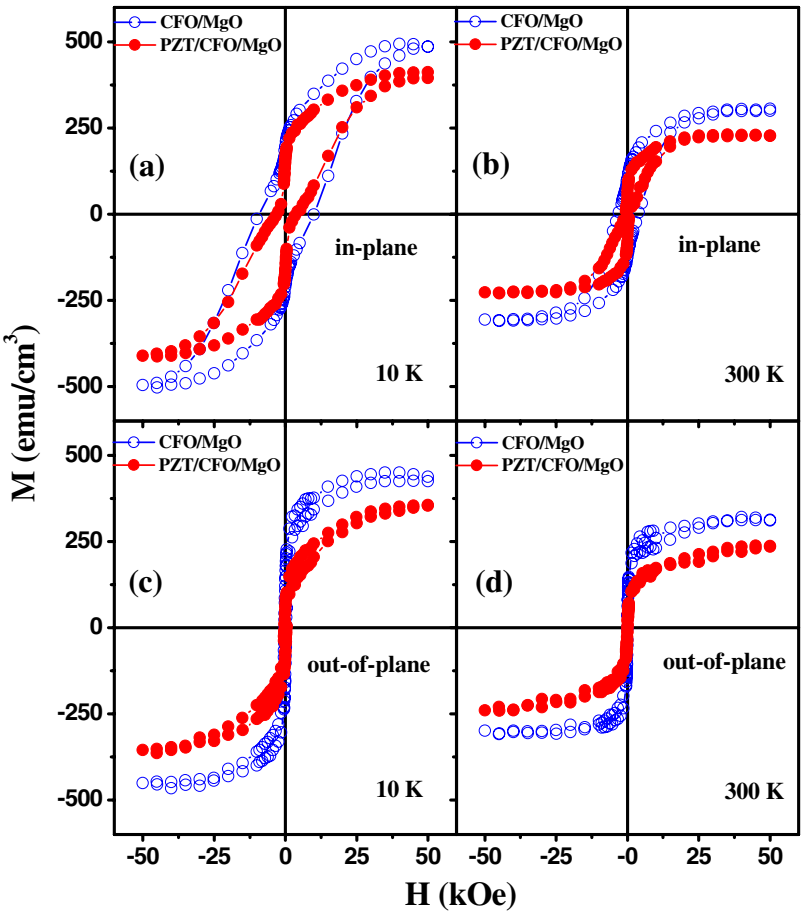

Figure 4. M–H loops measured at (a) and (c) 10 K and (b) and (d) 300 K for the CFO–MgO and PZT/CFO/MgO films, respectively. The in-plane and out-of-plane denote directions for the magnetic field applied parallel or perpendicularly to the film plane, respectively.

which could be reminiscent of epitaxial growth. Additionally, the grains appeared to be preferentially elongated in one of the in-plane orientations. This effect could be correlated with the larger difference in the $a_{\parallel}$ (8.294 Å) and $a_{\perp}$ (8.338 Å) values of the CFO layer in PZT/CFO/MgO (table 1). Figure 3(c) is a three-dimensional projection of the PZT top layer shown in figure 3(b). Films grown on STO substrates showed distinctively different surface morphologies. Figure 3(d) shows the surface of the CFO/STO film. The surface appears rougher than CFO/MgO with $R_{\rm rms}$ value of 7.502 nm. It also consisted of grains with various shapes and sizes. This could be attributed to the island growth mode [28, 29]. Figure 3(e) shows the PZT top surface for the PZT/CFO/STO film. The various grain sizes with larger grain growth and $R_{\rm rms}$ value of 22.683 nm still conformed to the island growth mechanism.

3.2. Magnetization measurements

Figure 4 shows the magnetization (M)–magnetic field (H) hysteresis loops for PZT/CFO/MgO and CFO/MgO, respectively. Similarly, figure 5 shows the M–H loops for PZT/CFO/STO and CFO/STO, respectively. The in-plane and out-of-plane configurations symbolized by $\parallel$ and $\perp$, respectively, represent the application of the magnetic fields parallel and perpendicular to the film planes. The hysteresis loops were acquired after the removal of the diamagnetic contribution from the substrates. In addition, since the thickness of CFO layer was kept constant in all the films, the magnetization values were only normalized to the volume of the CFO layer assuming no magnetic contribution from the PZT layer. Table 2 summarizes the saturation magnetization ($M_{\rm s}$), ratio of remanent magnetization ($M_{\rm r}$) to $M_{\rm s}$ and the coercivity ($H_{\rm c}$) for all the samples at 300 and 10 K. The $M_{\rm r}/M_{\rm s}$ ratio provides an estimate of the degree of squareness of the loops. The magnetic measurements were performed both at 300 and 10 K to emphasize the consistency of the underlying mechanisms.

The $M_{\rm s}$ values for CFO films on STO substrates were larger than those on MgO substrates [25]. The $M_{\rm s}$ value for the PZT/CFO/STO film was about 5.8$\mu_{\rm B}$ per Co^{2+} site which is much higher than the theoretical saturation value of 3$\mu_{\rm B}$ per Co^{2+} site [30]. This discrepancy between the theoretical and experimental values can be attributed to the distribution of Co^{2+} and Fe^{3+} cations in the CFO unit cell. In an inverse spinel structure of CFO, half of the octahedral coordination sites are occupied by Co^{2+} cations and the remaining half as well as all the tetrahedral coordination sites are occupied by the Fe^{3+} cations. The eight Fe^{3+} ions in tetrahedral sites are aligned antiferromagnetically with respect to the remaining eight Fe^{3+} ions via super-exchange interactions mediated by oxygen ions. Thus the uncompensated Co^{2+} ions which have three unpaired electrons in their d-orbitals would give

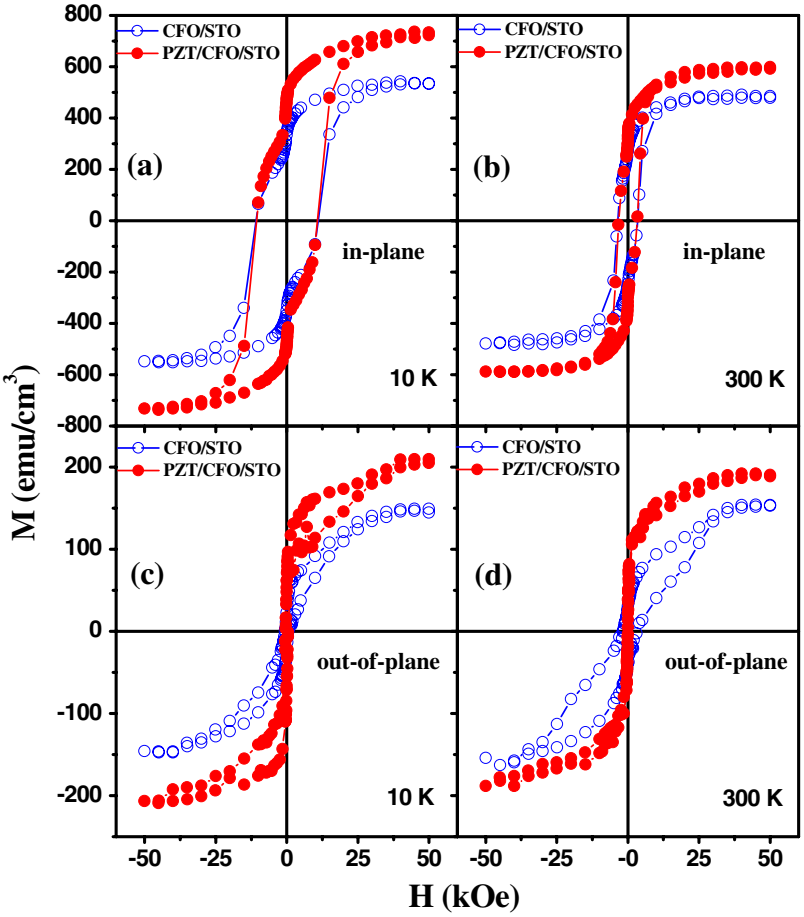

Figure 5. M–H loops measured at (a) and (c) 10 K and (b) and (d) 300 K for the CFO–STO and PZT/CFO/STO films, respectively. The in-plane and out-of-plane denote directions for the magnetic field applied parallel or perpendicularly to the film plane, respectively.

Table 2. Summary of saturation magnetization (M_s), ratio of remanent magnetization (M_r) to M_s and the coercivity (H_c) for CFO and CFO–PZT films on MgO and STO substrates measured at 300 K and 10 K. The in-plane and out-of-plane directions have been denoted by the symbols ∥ and ⊥, respectively.

Sample	$M_{s\parallel}$ (emu cm^{-3})	$M_{s\parallel}$ μ_B/Co^{2+}	$M_r/M_{s\parallel}$ (%)	$H_{c\parallel}$ (kOe)	$M_{s\perp}$ (emu cm^{-3})	$M_{s\perp}$ μ_B/Co^{2+}	$M_r/M_{s\perp}$ (%)	$H_{c\perp}$ (kOe)
300 K								
CFO/MgO	305 ± 4	2.4	37.6	3.8	310 ± 6	2.5	<13.9	<0.03
PZT/CFO/MgO	228 ± 2	1.8	25.8	1	234 ± 5	1.8	<5.9	<0.03
CFO/STO	478 ± 5	3.8	53.9	3.5	>164	>1.3	>21.6	3.0
PZT/CFO/STO	592 ± 5	4.7	53.6	3.4	190	1.5	41.5	0.1
10 K								
CFO/MgO	>497	>3.9	>41.3	10	441 ± 12	3.5	30.9	0.3
PZT/CFO/MgO	>400	>3.2	>39.6	4	353 ± 3	2.8	18.1	0.3
CFO/STO	541 ± 9	4.3	63.1	11	>164	>1.3	>14.6	0.7
PZT/CFO/STO	728 ± 9	5.8	65.6	11	206	1.6	28.8	0.5

a theoretical saturated magnetization value of $3\mu_B$ per Co^{2+} site [30]. Such a calculation neglects the contribution of the orbital motion of electrons. Further, the Fe^{3+} moments are assumed to be aligned perfectly anti-parallel although in reality they could be canted. The canting of the moments from the anti-parallel configuration and the change in cation distribution in the tetrahedral and octahedral sites, etc, can all alter the effective magnetic moment of CFO. These factors could be responsible for the enhanced magnetization in the PZT/CFO/STO film.

From figure 4 it could be observed that the magnetization of CFO reduced in the PZT/CFO/MgO film as compared with that in the CFO/MgO film both at 300 and 10 K. Around a 25% decrease in the M_s values was observed for the CFO/MgO film with the deposition of the PZT top layer both in the in-plane and out-of-plane directions at 300 K (see table 2). However, the H_c values still remained about the same. The out-of-plane anisotropy exhibited by the CFO/MgO film could be clearly seen in the M–H loops measured at 10 K (figures 4(a) and (c)). The in-plane magnetization did not show any

saturation even at 50 kOe while on the other hand the out-of-plane magnetization showed well-behaved saturation. This behaviour was preserved in the M–H loops of PZT/CFO/MgO films. This suggested that the easy axis of magnetization of the CFO/MgO film did not change with deposition of the PZT top layer. In short, the net effect of addition of the PZT layer on top of the CFO/MgO film was an observed decrease in magnetization with nominal change in coercivity and squareness.

In contrast, magnetization of the CFO/STO film increased with the addition of PZT on top as shown in figure 5. Around a 25% and 34% increase in the in-plane M_s could be estimated for PZT/CFO/STO at 300 K and 10 K, respectively (see table 2). The out-of-plane M_s also increased by 25% at 10 K in the PZT/CFO/STO film as compared with the CFO/STO film. The CFO/STO film exhibited strong in-plane anisotropy with well-saturated loops in the in-plane direction (figures 5(a) and (b)) and almost no saturation in the out-of-plane direction (figures 5(c) and (d)). However, from figure 5(d) it is evident that the out-of-plane magnetization at 300 K for PZT/CFO/STO showed well-saturated behaviour with an almost double M_r/M_s ratio (see table 2) compared with CFO/STO film. A similar trend was observed at 10 K (figure 5(c)). This could possibly indicate a reorientation in the direction of the easy axis of magnetization for the CFO/STO film with the deposition of the PZT top layer. Thus the net effect on the magnetic properties of the CFO/STO film with PZT top layer is an increase in magnetization and change in direction of magnetic anisotropy.

The effect of stress (σ) on the magnetization of a magnetostrictive material can be understood from the following thermodynamic relation [31]:

$$\frac{1}{l}\frac{\partial l}{\partial H} = \frac{\mu_o}{4\pi}\frac{\partial M}{\partial \sigma}, \tag{1}$$

where M is the magnetization, μ_o is the magnetic constant, σ is the stress, l is the length of the material and H is the external applied magnetic field. From equation (1) it is observed that the magnetization is decreased (increased) by tension (compression) if the magnetostriction ($\Delta l/l$) is negative (positive) when $\partial\sigma$ is positive (negative). Since CFO is a negative magnetostrictive material the magnetization would be reduced by stress (tensile).

The CFO/MgO film was under in-plane tensile stress (see table 1) due to the lateral stretching along the film plane which resulted in the $a_{\parallel}$ (8.403 Å) being larger than $a_{\perp}$ (8.386 Å). With the addition of a top PZT layer the in-plane residual stress might be increased which resulted in reduced magnetization in PZT/CFO/MgO. In contrast, the CFO/STO film was under large in-plane compressive stress with $a_{\perp}$ (8.494 Å) larger than $a_{\parallel}$ (8.292 Å). With the deposition of the PZT layer, the stress was released making the $a_{\parallel}$ (8.330 Å) in PZT/CFO/STO larger than that in CFO/STO. Thus strain relaxation enhanced the magnetization in the PZT/CFO/STO film. The results matched well with the negative magnetostriction of CFO.

4. Conclusions

In conclusion, epitaxial bilayers of CFO and PZT were successfully grown on single crystal substrates MgO and STO substrates by the PLD technique. The films grown on MgO (1 0 0) showed better in-plane epitaxy compared with the films grown on STO (1 0 0). In-plane strain on the CFO film grown on MgO increased with the deposition of PZT layer on top. This increase in stress in the CFO layer in PZT/CFO/MgO resulted in lowered saturation magnetization compared with the CFO/MgO film. In the case of the films grown on STO (1 0 0), the strain was already high in the CFO/STO film due to the larger film–substrate lattice mismatch. With the deposition of the PZT top layer the in-plane strain reduced slightly, which in turn resulted in higher saturation magnetization. Furthermore, the different values of magnetization of CFO for both single and bilayers films grown on STO and MgO substrates were influenced by the different degree of epitaxy on these substrates. The strain-modulated magnetism observed in these CFO–PZT bilayers suggested possible magnetoelastic coupling in these bilayers. This work provides useful insight into the role of interfacial stress in epitaxial CFO–PZT bilayers.

Acknowledgments

This work was supported in part by the National Science Foundation (Grant Nos DMI-0217939 and DMI-0078917) and the Department of Defense (Grant No W81XWH-07-1-0708). HS also acknowledges support from DOE through grant DE-FG02-06ER46275.

References

[1] Lee E W 1955 *Rep. Prog. Phys.* **18** 184–229
[2] Kneller E 1962 *Ferromagnetismus* (Berlin: Springer)
[3] Sander D 1999 *Rep. Prog. Phys.* **62** 809–58
[4] Jiles D C and Atherton D L 1984 *J. Phys. D: Appl. Phys.* **17** 1265–81
[5] Bozorth R M, Tilden E F and Williams A J 1955 *Phys. Rev.* **99** 1788
[6] Ranvah N, Nlebedim I C, Melikhov Y, Snyder J E, Jiles D C, Moses A J, Williams P I, Anayi F and Song S H 2008 *IEEE Trans. Magn.* **44** 3013
[7] Paulsen J A, Ring A P, Lo C C H, Snyder J E and Jiles D C 2005 *J. Appl. Phys.* **97** 044502
[8] Chen Y, Snyder J E, Dennis K W, McCallum R W and Jiles D C 2000 *J. Appl. Phys.* **87** 5798
[9] Inoue M, Yamamoto S, Fujita N and Fujii T 1987 *IEEE Trans. Magn.* **23** 3334
[10] Ramesh R and Spaldin N A 2007 *Nature Mater.* **6** 21–9
[11] Zheng H *et al* 2004 *Science* **303** 661
[12] Zhou J P, Qiu Z C and Liu P 2008 *Mater. Res. Bull.* **43** 3514
[13] Vopsaroiu M, Blackburn J and Cain M G 2007 *J. Phys. D: Appl. Phys.* **40** 5027–33
[14] Li Z, Wang Y, Lin Y and Nan C 2009 *Phys. Rev.* B **79** 180406(R)
[15] Sim C H, Pan Z Z and Wang J 2009 *J. Appl. Phys.* **105** 084113
[16] He H, Ma J, Lin Y and Nan C W 2008 *J. Appl. Phys.* **104** 114114
[17] He H C, Wang J, Zhou J P and Nan C W 2007 *Adv. Funct. Mater.* **17** 1333
[18] Zhou J P, He H C, Zhang Y, Deng C Y, Shi Z and Nan C W 2007 *Appl. Phys.* A **89** 553

[19] Zhou J P, He H, Shi Z and Nan C W 2006 *Appl. Phys. Lett.* **88** 013111
[20] Ortega N, Kumar A, Katiyar R S and Rinaldi C 2009 *J. Mater. Sci.* **44** 5127
[21] Zhang Y, Li Z, Deng C, Ma J, Lin Y and Nan C W 2008 *Appl. Phys. Lett.* **92** 152510
[22] Nan C, Bichurin M I, Dong S, Viehland D and Srinivasan G 2008 *J. Appl. Phys.* **103** 031101
[23] Zhang J X, Dai J Y and Chan H L W 2010 *J. Appl. Phys.* **107** 104105
[24] Eom C B, Van Dover R B, Phillips J M, Werder D J, Marshall J H, Chen C H, Cava R J, Fleming R M and Fork D K 1993 *Appl. Phys. Lett.* **63** 2570
[25] Dhakal T, Mukherjee D, Hyde R, Mukherjee P, Phan M H, Srikanth H and Witanachchi S 2010 *J. Appl. Phys.* **107** 053914
[26] Hirata K, Moriya K and Waseda Y 1977 *J. Mater. Sci.* **12** 838
[27] Meyer G M, Nelmes R J and Hutton J 1978 *Ferroelectrics* **21** 461
[28] Huang W, Zhu J, Zeng H Z, Wei X H, Zhang Y and Li Y R 2006 *Appl. Phys. Lett.* **89** 262506
[29] Huang W, Zhou L X, Zeng H Z, Wei X H, Zhu J, Zhang Y and Li Y R 2007 *J. Cryst. Growth* **300** 426
[30] Bozorth R M 1961 *Ferromagnetism* (New York: D. Van Nostrand Company, Inc.) 6th edn
[31] Jiles D C 1995 *J. Phys. D: Appl. Phys.* **28** 1537